Int. J. Electrochem. Sci., 16 **(2021)** Article ID: 210665, doi: 10.20964/2021.06.64

International Journal of
ELECTROCHEMICAL
SCIENCE
www.electrochemsci.org

Effect of temperature on corrosion behavior of X70 pipeline steel in 3.5% NaCl solution

Meijun Wu, Zhiming Gao[*], *Shixiong Wu, Yingjie Liu, Wenbin Hu*

Tianjin Key Laboratory of Composite & Functional Materials, School of Materials Science and Engineering, Tianjin University, Tianjin, 300072, China
[*]E-mail: gaozhiming@tju.edu.cn

Received: 2 March 2021 / *Accepted:* 19 April 2021 / *Published:* 30 April 2021

Effect of temperature on the corrosion behavior of X70 pipeline steel in 3.5% NaCl solution was studied by the immersion test, polarization curves, electrochemical impedance spectroscopy (EIS), scanning electron microscope (SEM), and X-ray diffraction (XRD). The corrosion potential (E_{corr}) decreases, and the corrosion current density (I_{corr}) increases with the increase of temperature, so the corrosion rate increases. With the increase of temperature, the size of the capacitive semicircle of the Nyquist plots and the modulus of the impedance decreases at the same immersion time. Moreover, the characteristic frequency in the phase Angle plots decreases. The double charge layer capacitance (Q_{dl}) increases with the increase of temperature and the immersion time. With the increase of temperature, the solution resistance (R_s), the charge transfer resistance (R_t) and the adsorption resistance of the corrosion product (R_f) decreases, the adsorption capacitance of the corrosion product (Q_f) increases, the surface of the X70 steel was covered by a large amount of the gathered corrosion products, and the amount and the size of corrosion products significantly increases. With the increase of immersion time, R_t, the trend of the modulus of the impedance at low frequency, and R_f decreases at 25°C, 40°C, and 60°C, a small amount of corrosion products covered the surface of the X70 steel and more cracks were appeared on the corrosion products. However, at 80°C and 95°C, these increases, a large amount of corrosion products covered the surface of the X70 steel, which is consistent with the increase of R_f that inhibits the corrosion process. At different temperatures and immersion time, the main composition of the corrosion products is similar, with Fe_3O_4, FeOOH and Fe_2O_3.

Keywords: X70 pipeline steel; Temperature; Immersion test; Corrosion behavior; EIS.

1. INTRODUCTION

The marine environment contains numerous marine resources, such as oil, gasoline, diesel, liquefied natural gas and minerals. In recent years, with the rapid increase of energy consumption, the demand for high-strength low alloy steel in marine exploration is increasing [1]. To ensure the development and transportation of oil and gas, a large number of low alloy and high strength steels are used in submarine pipeline steels [2]. Because of the high strength and toughness, X70 pipeline steel has become the steel used in China's west-to-east gas pipeline [3-6]. In fact, the marine environment is a complex system, and many factors affect the corrosion behavior, such as temperature, hydrostatic pressure, flow velocity, PH, and so on [7]. The transportation of heavy oil takes place at high temperatures.

Previous studies have shown that temperature has an obvious effect on the corrosion behavior of various metals or alloys [8-11]. As the temperature of the medium increases, the corrosion potential moves to a negative value, the corrosion current density moves to a positive value, which shows that the pipeline steel has higher activity in the solution [12]. Meanwhile, in the corrosion process of pipeline steel, the temperature has a significant influence on the anodic and cathodic reaction of Tafel [13-15]. With the increase of temperature, corrosion products, pitting and cracks appear on the surface of steel [16, 17]. Temperature speeds up the activity of ions, increasing the corrosion rate of steel [18, 19]. The immersion time also has an important effect on the corrosion behavior of pipeline steel [20-22]. Studies have shown that X65 steel corrodes during initial immersion in seawater containing sulfate-reducing bacteria in an anaerobic environment. With the extension of immersion time, the biofilm was formed and the corrosion process was inhibited [23].

In this study, the effect of temperature on the corrosion behavior of X70 pipeline steel in 3.5% NaCl solution was investigated using immersion test, polarization curves, electrochemical impedance spectroscopy (EIS), scanning electron microscopy (SEM), and X-ray diffraction (XRD) tests. The purpose of this study is to investigate the corrosion behavior in simulated high temperature environment. It has more primary value in the field of the corrosion of pipeline steel and provides a new insight into the study on the corrosion of pipeline steel in high temperature environment in the future.

2. EXPERIMENTAL

2.1Materials and preparation

The test solution used in this study was 3.5% NaCl solution. The experimental material used in this study was X70 pipeline steel, with the chemical composition (wt.%) of 0.06 C, 1.54 Mn, 0.38 Si, 0.15 Cr, 0.02 P, 0.002 S, 0.031 Ni, 0.29Mo, 0.005 V and Fe balance. The size of the samples was 10 mm × 10 mm×3 mm. The copper wire was weld on the back of the samples, and then sealed samples with epoxy resin. The working area was 1cm^2. The surfaces of the specimens were polished from 80# to 1500# by SiC paper, and then washed with distilled water and degreased with anhydrous ethanol. The temperature of the solution was controlled at 25℃, 40℃, 60℃, 80℃, 95℃ by using a constant temperature water bath.

2.2 Immersion test and Electrochemical measurements

The immersion tests were carried out at 25℃, 40℃, 60℃, 80℃, 95℃ for one day, two days, three days, five days and eight days. The electrochemical tests were performed using an electrochemical workstation (PARSTAT 2273) in a three-electrode system. The reference electrode (RE) was a saturated calomel electrode (SCE) with a salt bridge (at room temperature), the working electrode (WE) was the X70 steel, the counter electrode (CE) was a platinum electrode (Pt). At a steady-state open circuit potential (OCP), the cathodic polarization curves of X70 steel were measured from the $\mathrm{OCP}_{\mathrm{vs.\ SCE}}$ to -0.6 $\mathrm{V}_{\mathrm{vs.\ OCP}}$, the anodic polarization curves were measured from $\mathrm{OCP}_{\mathrm{vs.\ SCE}}$ to 0.5 $\mathrm{V}_{\mathrm{vs.\ OCP}}$ at a scan rate of 0.5 mV/s. EIS was measured at OCP using the amplitude of the AC sine wave signal of 10 mV in the scanning frequency range of 100 kHz to 10 mHz. All EIS data were fitted by Zsimpwin software using the equivalent circuit model.

2.3 Surface and phase analysis

The morphologies of the corrosion product immersed for five and eight days were investigated by scanning electron microscopy (SEM) (S4800, Japan) with an accelerating voltage of 15 kV. And the phase composition of the surface corrosion products was examined by X-ray diffraction (XRD) (D8 Advance, Bruker, Germany) with CuK_{α} radiation, and 2θ ranged from 5° to 120°, with a 0.02° step, and a 4 s count time at each step. The results were analyzed using Jade V6.5 software.

3. RESULTS AND DISCUSSION

3.1 Potentiodynamic polarization curves

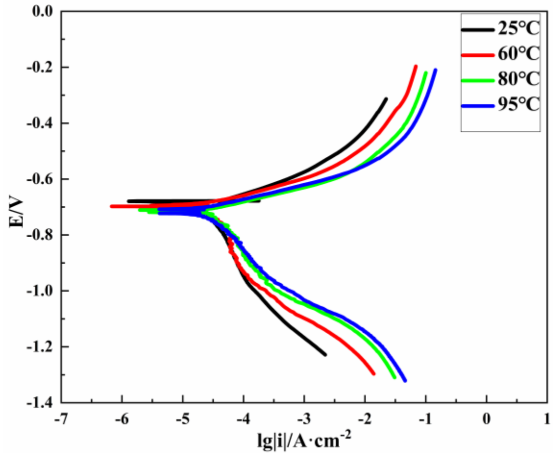

Figure 1. Polarization curves of X70 steel in 3.5% NaCl solution at different temperatures.

Table 1. Corrosion potential and corrosion current density of X70 steel at different temperatures

Temperature/℃	25	60	80	95
E_{corr}/mV	-678	-696	-711	-722
I_{corr}/A·cm^{-2}	1.072×10^{-4}	1.349×10^{-4}	1.585×10^{-4}	1.660×10^{-4}

Fig.1 shows the polarization curves of X70 steel in 3.5% NaCl solution at different temperatures. Table 1 shows the corrosion potential and corrosion current density of X70 steel at different temperatures. As can be seen from Fig.1 and Table 1, with the increase of temperature, the corrosion potential E_{corr} decreases, and the corrosion current density I_{corr} increases. Because the kinetics of the electrochemical reactions increases with the increase of temperature [24-26], which suggests that the corrosion rate increases. It could be attributed to the enhancement of the diffusion of ions [27].

As shown in Fig.1, the slope for the cathodic polarization curves increases with the increase of temperature. It suggests that the cathodic process of oxygen diffusion is obvious at low temperature, while the mass-transfer rate is accelerated with the increase of temperature [28], so that the cathodic process of oxygen diffusion is less obvious.

The activation energy of the corrosion process can be calculated from the Arrhenius relationship and the corrosion current density from Table 1 as equation:

$$\log(I_{corr}) = \log A - \frac{E_a}{2.303RT} \qquad (1)$$

where E_a, T, A, R and are the apparent activation corrosion energy, the absolute temperature, the Arrhenius constant, and the gas constant of 8.314 J•mol^{-1}•K^{-1} respectively.

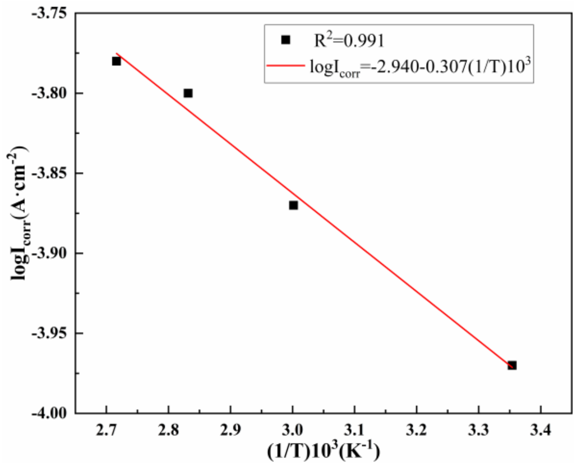

Figure 2. Arrhenius plots of X70 steel in 3.5% NaCl solution at different temperatures.

Fig.2 provides an indication of the dependence of the corrosion current density I_{corr} on the temperature. The value of E_a is obtained from the Arrhenius plots shown in Fig.2, which is 5.878 kJ/mol. As can be seen from Fig.2, the relationship between log (I_{corr}) and 1/T is linear [29-31], demonstrating that I_{corr} increases with the increase of temperature, and the corrosion rate increases.

3.2 Electrochemical impedance spectroscopy measurements

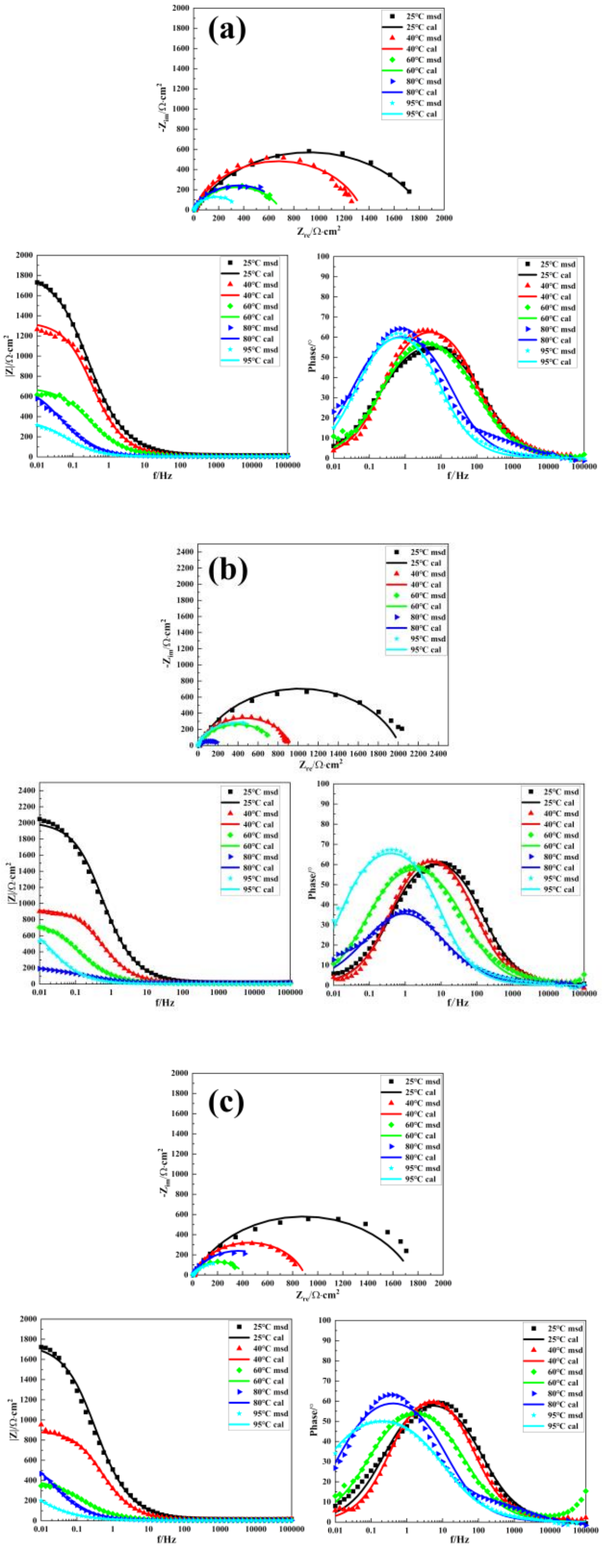

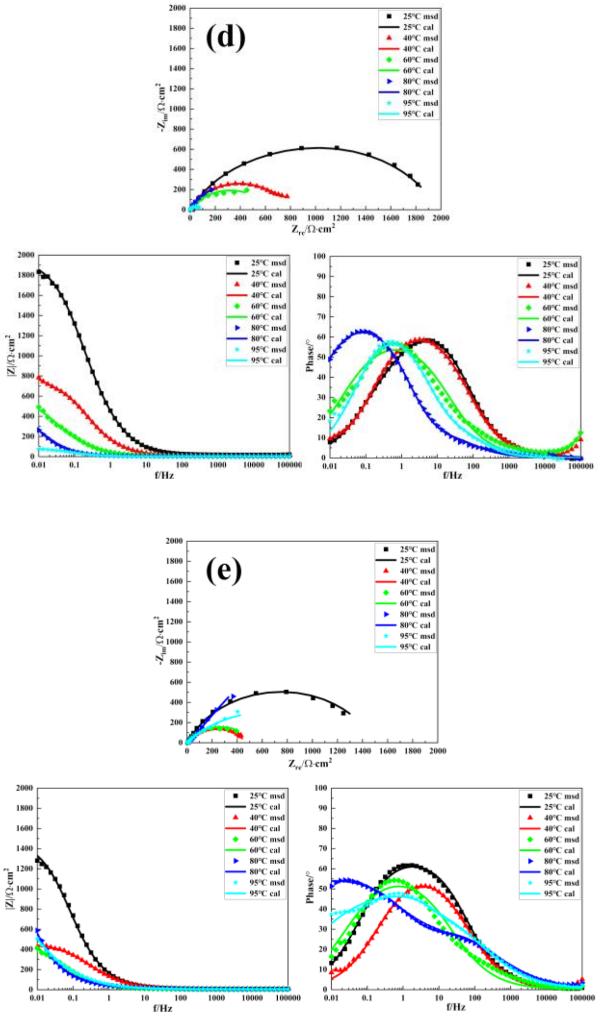

Figure 3. Electrochemical impedance spectroscopy (EIS) in 3.5% NaCl solution at different temperatures after immersion for: (a) 1 day; (b) 2 days; (c) 3 days; (d) 5 days; (e) 8 days.

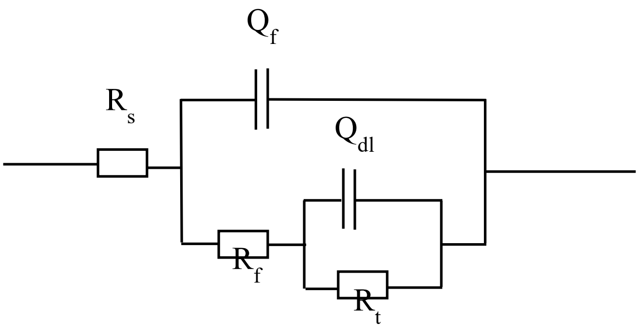

Figure 4. The equivalent circuit for the EIS results.

As shown in Fig. 4, the equivalent circuit model corresponds to a simple corrosion system, in which R_s, R_f and R_t represent the solution resistance from the reference electrode to the working electrode, the adsorption resistance of the corrosion product and the charge transfer resistance of the electrode reaction, and Q_{dl} and Q_f represent the double charge layer capacitance on the electrode surface and the adsorption capacitance of the corrosion product, respectively [32]. Taking into account that the surface roughness, dislocations or grain boundaries leads to the nonuniformity of the surface [33], the pure capacitor C is replaced by the constant phase angle element Q, n means the exponent ranging from -1 to 1.

Fig.3 shows that with the increase of temperature, the size of the capacitive semicircle of the Nyquist plots and the modulus of the impedance decreases at the same immersion time. The size of the capacitive semicircle of the Nyquist plots is a reflection of the resistance in the electrochemical process. Therefore, it suggests that the corrosion rate increases with the increase of temperature, which could be attributed to the increase of the diffusion ability of corrosive ions, and the increase of the rate of metal dissolution and oxidation-reduction reaction [34]. Meanwhile, the characteristic frequency in the phase Angle plots decreases with the increase of temperature.

Table 2. Fitting results for the EIS data of X70 steel at different temperatures and different immersion time.

Immersion time(day)	Temperature (℃)	R_s ($\Omega\cdot cm^2$)	Q_f ($\mu F\cdot cm^{-2}$)	n	R_f ($\Omega\cdot cm^2$)	Q_{dl} ($\mu F\cdot cm^{-2}$)	n	R_t ($\Omega\cdot cm^2$)
1	25	16.24	374.71	0.7583	46.91	224.51	0.7313	1002.00
1	40	10.31	205.76	0.8929	25.24	305.21	0.7997	1265.00
1	60	7.15	554.45	0.8209	14.58	652.95	0.6995	661.00
1	80	4.66	2352.10	0.7134	4.60	2219.10	0.8997	639.10
1	95	4.64	1470.02	0.9290	1.46	2821.02	0.7934	343.46
2	25	12.22	61.93	0.9573	36.06	237.11	0.6286	1034.00
2	40	9.96	258.16	0.8944	35.29	470.95	0.7818	865.71
2	60	7.13	250.82	0.9457	3.79	891.03	0.7423	661.57
2	80	4.34	577.25	0.6575	1.52	2614.20	0.8279	516.92
2	95	3.98	2151.06	0.7829	6.07	3325.08	1	373.17
3	25	11.61	308.26	0.8137	35.60	814.47	0.5856	1206.00
3	40	9.52	134.28	1	20.11	913.95	0.7295	855.88
3	60	6.73	1741.30	1	5.15	979.46	0.7171	409.60
3	80	4.06	1789.14	0.8025	3.03	2814.00	0.8057	597.00
3	95	3.87	2504.00	0.8073	4.76	3803.00	0.6093	430.36
5	25	11.22	433.14	0.7842	26.86	1113.00	0.6956	967.87
5	40	8.53	1331.00	0.7596	16.62	1243.00	1	1066.00
5	60	5.33	2066.06	0.6899	10.17	1875.00	0.8534	510.68
5	80	4.18	2746.01	0.7856	2.23	2945.00	0.7978	685.34
5	95	3.54	3724.00	0.8933	0.88	4267.00	0.7679	85.23
8	25	10.32	970.00	0.7909	23.57	1464.13	0.7543	715.21
8	40	7.79	1360.00	1	8.30	1789.00	0.7157	455.28
8	60	5.23	2400.00	0.7287	6.52	3890.00	0.7586	437.44
8	80	3.78	3053.00	0.5815	29.92	4150.01	0.6664	1867.72
8	95	3.12	4537.00	0.5524	15.17	4286.00	1	656.65

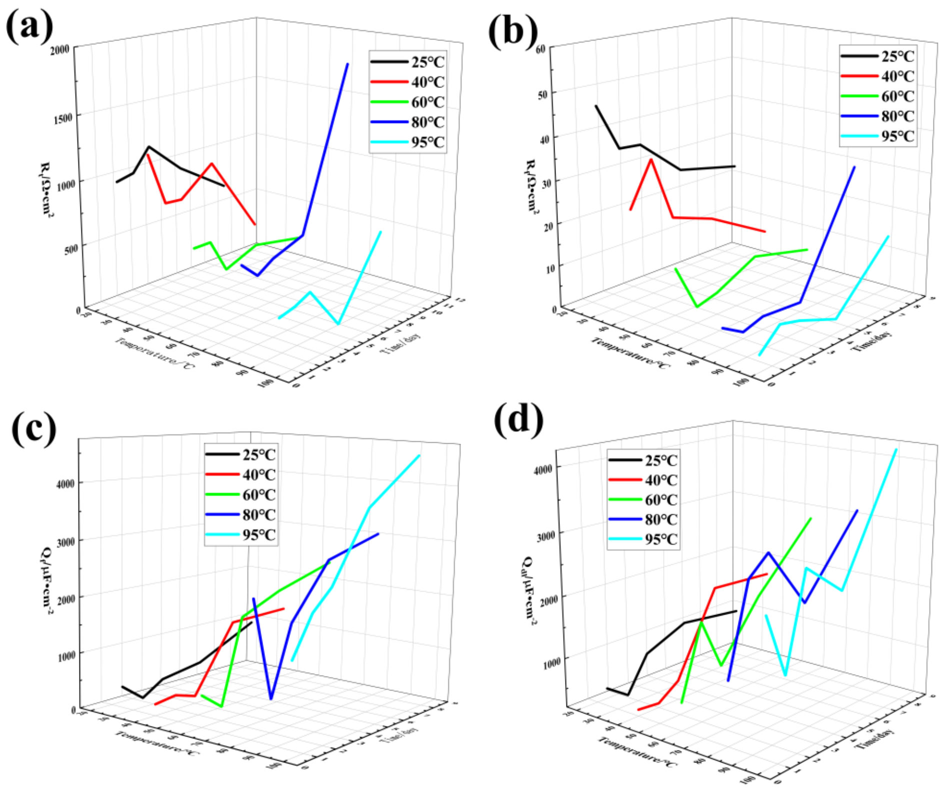

Figure 5. the parameters of the fitting results at different temperatures and different immersion time: (a) R_t, (b) R_f, (c) Q_f, (d) Q_{dl}.

The fitting results for the EIS data of X70 steel at different temperatures and different immersion time are illustrated in Table 2 and Fig.5. R_s decreases with the increase of temperature, indicating that the increase of temperature leads to the enhancement of ion activity and the tendency of the adsorption of Cl^-. With the increase of temperature, R_t decreases and Q_{dl} increases, which leads to the increase of the corrosion rate. It may be attributed to the increase of the electrochemical activity of X70 steel. Moreover, Q_f increases with the increase of temperature due to the increase of the defects in the corrosion product film of X70 steel. However, R_f decreases with the increase of temperature, which could be attributed to the detachment of a small amount of the corrosion products from the surface of X70 steel [35].

As illustrated in Fig.5, Q_{dl} also increases with the increase of immersion time, indicating that the roughness of the electrode surface becomes larger. At 25°C, 40°C, and 60°C, with the increase of immersion time, the decrease of R_t and R_f leads to the increase of the corrosion rate. However, at 80°C and 95°C, with the increase of immersion time, R_t increases and the surface electrochemical activity reduces leading to a decrease in corrosion resistance. At 80°C and 95°C, R_f increases with the increase of immersion time, which suggests that a denser corrosion product layer is formed on the surface of X70 steel. It is a barrier for diffusion and inhibits the process of the electrochemical reaction. Therefore, the corrosion resistance increases. Furthermore, with the increase of immersion time, the decrease of the content of dissolved oxygen may result in a decrease in the corrosion rate.

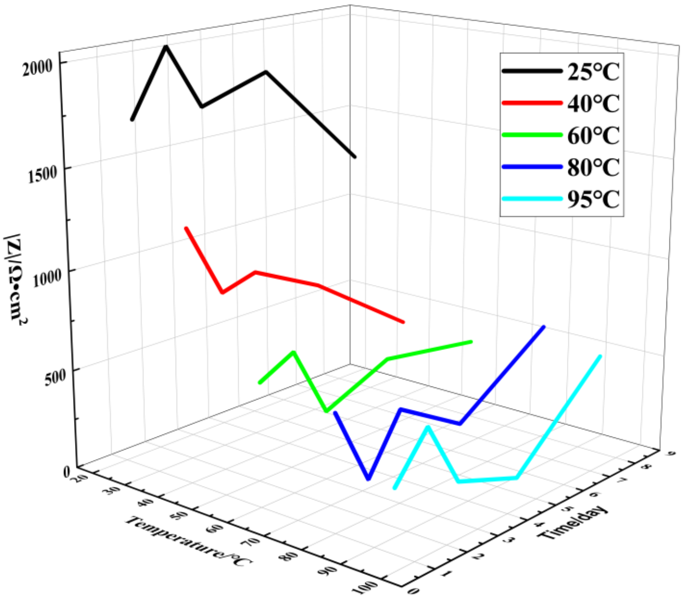

Figure 6. The modulus of the impedance of X70 steel at low frequency under different temperatures and immersion time.

The solution resistance in the low frequency region is very small, so the modulus of the impedance at low frequency in the Bode plots can reflect the corrosion resistance. A larger value of the modulus of the impedance at low frequency indicates a higher corrosion resistance of X70 steel. As can be seen from Fig.6, with the increase of temperature, the modulus of the impedance at low frequency decreases. It indicates that the corrosion rate increases, which could be related to the increase of the surface activity of the X70 steel and the enhancement of the diffusion of Cl^- in the solution. With the extension of immersion time, the trend of the modulus of the impedance at low frequency is decreasing at 25 °C, 40 °C, and 60 °C. Thus, the extension of time could have a significant influence on the corrosion process that leads to an increase of the corrosion rate. While with the extension of immersion time, the trend of the modulus of the impedance at low frequency is increasing at 80 °C and 95 °C, which could be attributed to the formation of the corrosion product film on the surface of X70 steel. The corrosion product film has a good adhesion and a compact structure so that the dissolved oxygen in the solution is prevented from contacting with the surface of X70 steel matrix [36], which leads to an increase of the corrosion resistance. Furthermore, at 80 °C and 95 °C, the extension of immersion time could lead to the decrease of the content of dissolved oxygen in the solution, which can inhibit the electrochemical corrosion process.

3.3 SEM results of corrosion products

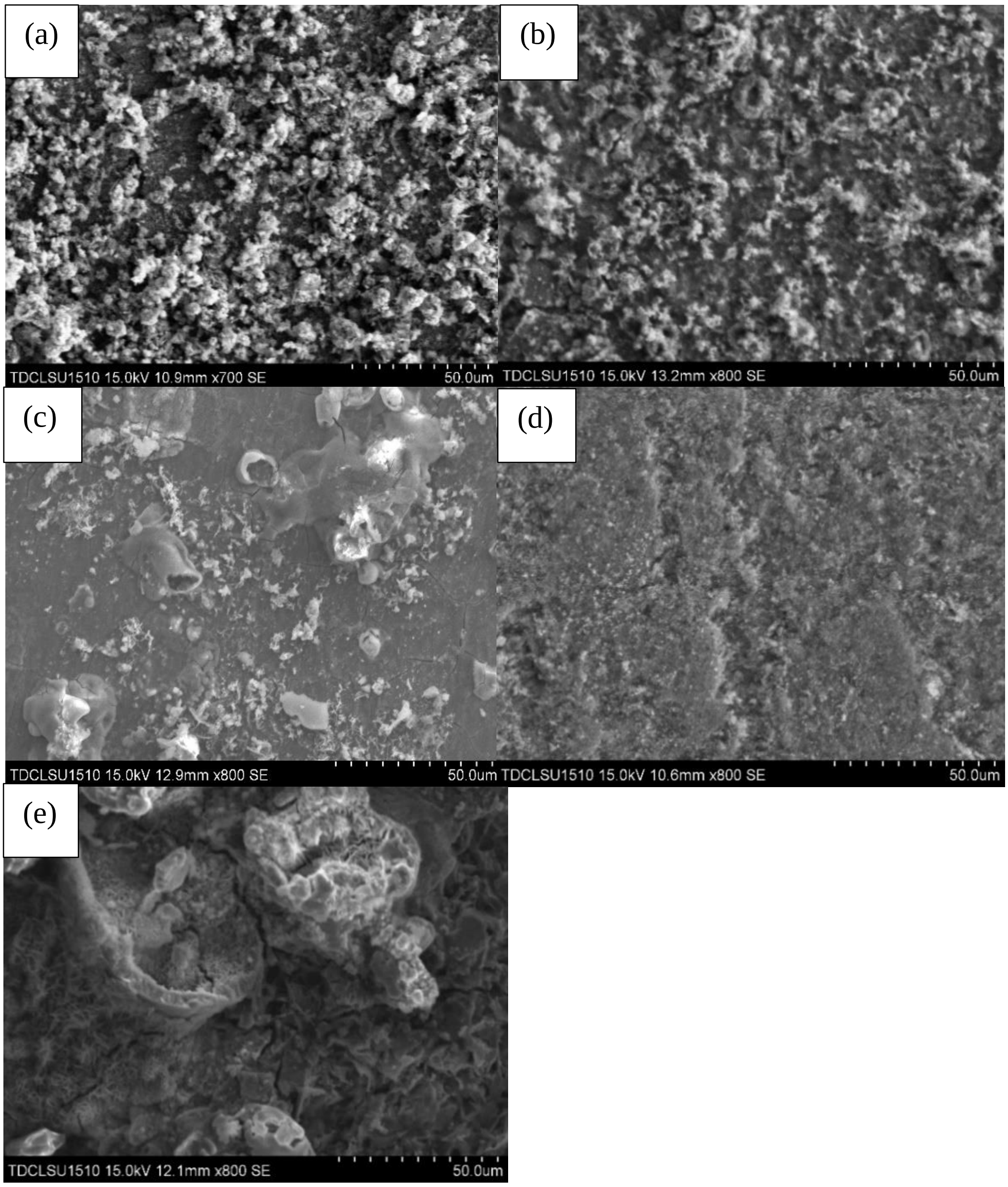

Figure 7. SEM images of the corrosion product film on X70 steel after immersion in 3.5% NaCl solution for 5 days: (a)25℃; (b) 40℃; (c) 60℃; (d) 80℃; (e) 95℃.

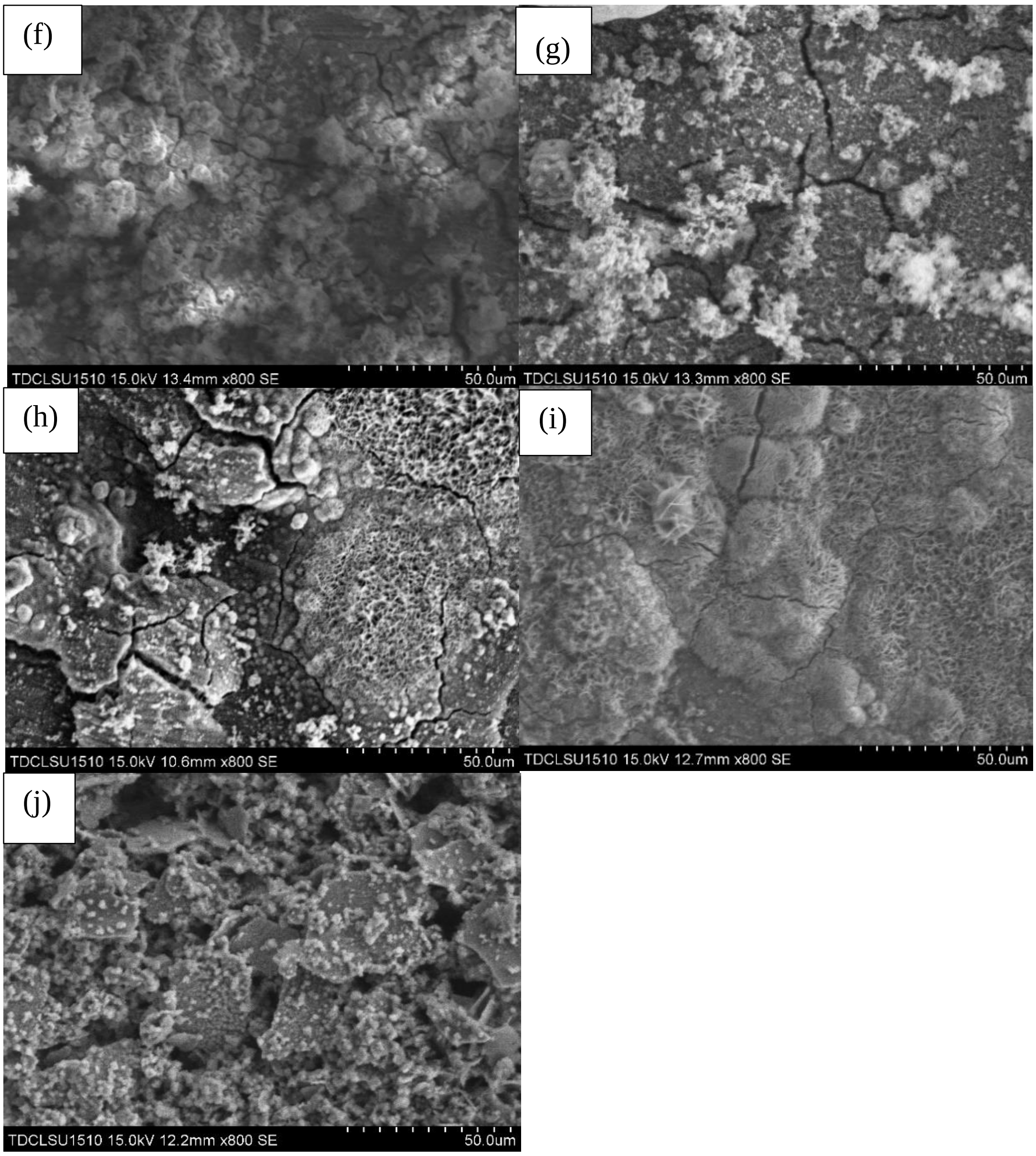

Figure 8. SEM images of the corrosion product film on X70 steel after immersion in 3.5% NaCl solution for 8 days: (f)25℃; (g) 40℃; (h) 60℃; (i) 80℃; (j) 95℃.

Fig.7-8 shows the SEM results of the corrosion products of X70 steel after immersion for 5 days and 8 days in 3.5% NaCl solution at different temperatures. With the increase of temperature, the surface of the X70 steel was covered by a large amount of the gathered corrosion products, the roughness of the steel increased, the amount and the size of corrosion products significantly increased. It is consistent with the increase of Q_{dl}. Thus, the corrosion rate increases with the increase of temperature, which is consistent with the results of R_t.

Fig.7-8 shows that at 25 ℃, 40 ℃, and 60 ℃, a small amount of corrosion products covered the surface of the X70 steel unevenly with the extension of immersion time. Moreover, more cracks were appeared on the corrosion products with the extension of immersion time, which provide a chance for the corrosive medium to reach the surface of the X70 steel [37]. Therefore, at 25 ℃, 40 ℃, and 60 ℃, the corrosion rate increases with the extension of immersion time. However, at 80 ℃ and 95 ℃, the surface of the X70 steel was covered by gathered corrosion products. Furthermore, the number of corrosion products increased significantly, which is consistent with the change of R_f. The thicker of the corrosion products leads to the increase of the migration resistance of reactive ions, so the protective effect of the corrosion product film on the matrix is enhanced, which inhibits the diffusion of dissolved oxygen to the X70 steel [38]. Thus, the corrosion rate decreases. Hence, with the increase of temperature and with the extension of immersion time, the SEM results are consistent with the EIS results.

3.4 XRD results of corrosion product

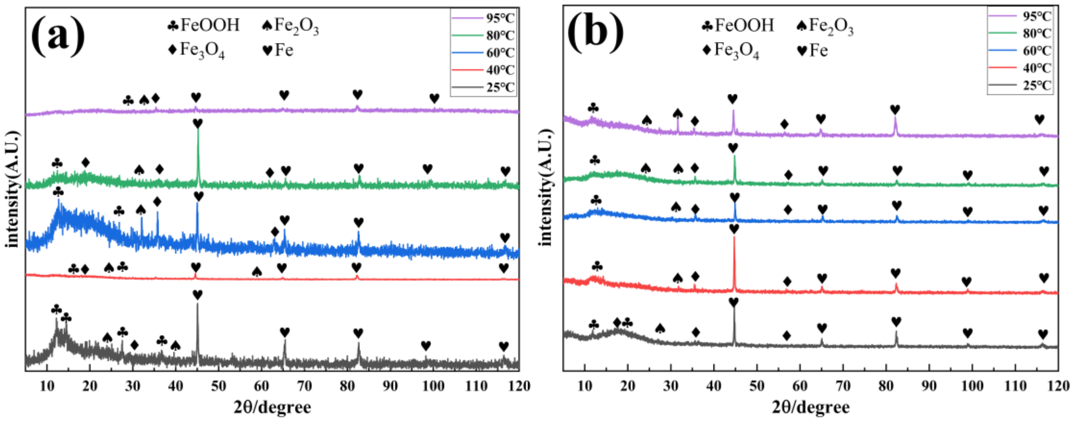

Figure 9. XRD analysis results of X70 steel in 3.5% NaCl solution at different temperatures after immersion for (a) 5 days; (b) 8 days.

Fig.9 shows the XRD results of the corrosion products of X70 steel after immersion for 5 days and 8 days in 3.5% NaCl solution at different temperatures. XRD results show that the corrosion products are similar at different temperatures and immersion time, with the main composition of Fe_3O_4, FeOOH and Fe_2O_3. In addition, Fe was found on the surface of X70 steel at different temperatures and immersion time, which demonstrates that the corrosion products were not completely covered on the surface of X70 steel. At the initial stage of immersion, the ions and the dissolved oxygen in the solution lead to the destruction of the metal matrix, which promotes the dissolution of iron [39]. However, with the extension of immersion time, the consumption of the dissolved oxygen leads to the formation of the corrosion product film on the surface of X70 steel. The brown-yellow outer layer corrosion product film was a composition of FeOOH and Fe_2O_3. With the extension of immersion time, a black inner corrosion product film with close adhesion to the matrix was formed on the surface of metal [40,41], with a composition of Fe_3O_4. In addition, it inhibits the contact of the corrosion medium and the surface, which leads to the reduction of corrosion rate with the extension of immersion time.

4. CONCLUSIONS

(1) The corrosion potential E_{corr} decreases, and the corrosion current density I_{corr} increases with the increase of temperature, which suggests that the corrosion rate increases.

(2) With the increase of temperature, the size of the capacitive semicircle of the Nyquist plots and the modulus of the impedance decreases at the same immersion time. Thus, the corrosion rate increases with the increase of temperature, which could be related to the increase of the diffusion ability of corrosive ions and the rate of metal dissolution and oxidation-reduction reaction. Moreover, the characteristic frequency in the phase Angle plots decreases with the increase of temperature.

(3) Q_{dl} increases with the increase of temperature and the immersion time. With the increase of temperature, R_s, R_t, the trend of the modulus of the impedance at low frequency, and R_f decreases, Q_f increases. With the increase of immersion time, R_t, the trend of the modulus of the impedance at low frequency, and R_f decreases at 25℃, 40℃, and 60 ℃. However, at 80℃ and 95℃, these increases, which leads to the decrease of corrosion rate.

(4) With the increase of temperature, the surface of the X70 steel was covered by a large amount of the gathered corrosion products. Furthermore, the amount and the size of corrosion products significantly increased.

(5) With the extension of immersion time, more cracks have appeared on the corrosion products, so the corrosion rate increases at 25 ℃, 40 ℃, and 60 ℃. However, the corrosion rate decreases at 80 ℃ and 95 ℃, which could be related to the change of R_f that the formation of the larger amount of corrosion products.

(6) The corrosion products are similar at different temperatures and immersion time, with the main compositions of Fe_3O_4, FeOOH and Fe_2O_3.

ACKNOWLEDGEMENTS
This work was supported by National Natural Science Foundation of China (No.51871164, No.51671144), Tianjin Science and Technology Project (No.20YDTPJC01780, No.18YFZCGX00050) and Shandong Taishan Industry Leading Talents Project (No. SF1503302301).

References

1. L.C. Yan, Y.P. Diao, Z.Y. Lang, K.W. Gao, *Sci. Technol. Adv. Mat.*, 21 (2020) 359.
2. G. Wang, L. Yin, Z. Yao, J. Wang, S. Jiang, Z. Zhang, C. Zuo, *Materials*, 12 (2019) 1762.
3. S. Hasan, L. Sweet, J. Hults, G. Valbuena, B. Singh, *Int. J. Pres. Ves. Pip.*, 159 (2018) 1.
4. Y.S. Yang, F. Khan, P. Thodi, R. Abbassi, *Reliab. Eng. Syst. Safe.*, 159 (2017) 214.
5. A. Vasseghi, E. Haghshenas, A. Soroushian, M. Rakhshandeh, *Eng. Fail. Anal.*, 119 (2021) 105009.
6. A. Del-Pozo, A. Torres-Islas, J.C. Villalobos, A. Sedano, H. Martinez, B. Campillo, S. Serna, *Corros. Eng. Sci. Techn.*, 54 (2019) 37.
7. X.H. Wang, L. Fan, K.K. Ding, L.K. Xu, W.M. Guo, J. Hou, T.G. Duan, *J. Mater. Sci. Technol.*, 64 (2021) 187.
8. J. Gao, J.B. Tan, Z.Y. Zhang, M. Jiao, X.Q. Wu, L.C. Tang, Y.F. Huang, *Corros. Sci.*, 180 (2021) 109196.
9. H.H. Sheu, Y.R. Chen, M.D. Ger, *Int. J. Electrochem. Sci.*, 15 (2020) 2851.
10. J. Ma, F. Feng, B.Q. Yu, H.F. Chen, L.F. Fan, *Int. J. Min. Met. Mater.*, 27 (2020) 347.

11. Z. Wang, Z. Feng, L. Zhang, *Corros. Sci.*, 174 (2020) 108844.
12. Y.C. Qing, Y.L. Bai, J. Xu, T.Q. Wu, M.C. Yan, C. Sun, *Materials*, 12 (2019) 144.
13. J. Qiu, Y.H. Li, Y. Xu, A.J. Wu, D.D. Macdonald, *Corros. Sci.*, 175 (2020).
14. B.C. Nielsen, O.N. Dogan, B.H. Howard, *Corros. Sci.*, 96 (2015) 74.
15. H.S. Chen, R. Tang, C.S. Long, G. Le, *Corros. Sci.*, 161 (2019) 108188.
16. S. Sharifi-Asl, F.X. Mao, P. Lu, B. Kursten, D.D. Macdonald, *Corros. Sci.*, 98 (2015) 708.
17. E. Mahdi, A. Rauf, E.O. Eltai, *Corros. Sci.*, 83 (2014) 48.
18. Q. Yan, Q. Yin, J. Cui, X.Y. Wang, Y.X. Qiao, H.L. Zhou, *Mater. Res. Express.*, 8 (2021) 016528.
19. Z.Y. Zhang, J.B. Tan, X.Q. Wu, E.H. Han, W. Ke, J.C. Rao, *Corros. Sci.*, 146 (2019) 80.
20. M. Baig, H.R. Ammar, A.H. Seikh, M.A. Alam, N.H. Alharthi, *Int. J. Electrochem. Sci.*, 12 (2017) 3336.
21. H.X. Liu, B.Y. Hu, Y. Chen, Y.W. Liu, Y. Xie, L. Zhang, Z.N. Yang, *Int. J. Electrochem. Sci.*, 13 (2018) 6201.
22. M.K. Keshavarz, A. Fattah-Alhosseini, *J. Mater. Eng. Perform.*, 27 (2018) 3386.
23. Q.S. Li, J.H. Wang, X.T. Xing, W.B. Hu, *Bioelectrochemistry.*, 122 (2018) 40.
24. B. Dong, X.D. Wen, L. Feng, *Int. J. Electrochem. Sci.* 15 (2020) 10844.
25. L. Simoni, J.Q. Caselani, L.B. Ramos, R.M. Schroeder, C.D. Malfatti, *Corros. Sci.*, 118 (2017) 178.
26. L.Q. Wang, Z.M. Gao, Y.J. Liu, X.B. Lu, C. Wang, W.B. Hu, *Int. J. Electrochem. Sci.*, 14 (2019) 161.
27. L. Caceres, T. Vargas, M. Parra, *Electrochim. Acta.*, 54 (2009) 7435.
28. J. Zhao, D. Xiong, Y.H. Gu, Q.F. Zeng, B. Tian, *J. Petrol. Sci. Eng.*, 173 (2019) 1109.
29. W.W. Kang, Z.M. Gao, Y.J. Liu, L.Q. Wang, *Int. J. Electrochem. Sci.*, 14 (2019) 2216.
30. Y.J. Liu, Z.M. Gao, X.B. Lu, L.Q. Wang, *Int. J. Electrochem. Sci.*, 14 (2019) 150.
31. J.X. Yu, H.K. Wang, Y. Yu, Z. Luo, W.D. Liu, C.M. Wang, *Corros. Sci.*, 133 (2018) 276.
32. M. Zhu, J. Ma, Y.F. Yuan, S.Y. Guo, *Int. J. Electrochem. Sci.*, 14 (2019) 9711.
33. Y.F. Cheng, *Int. J. Hydrogen. Energ.*, 32 (2007) 1269.
34. Y. Teng, D.Y. Sun, S. Wang, Y.S. Wang, Z.Y. An, Y. Li, X.L. Qu, X.D. Zhao, *Int. J. Electrochem. Sci.*, 14 (2019) 10670.
35. C.F. Dong, K. Xiao, Z.Y. Liu, W.J. Yang, X.G. Li, *Int. J. Min. Met. Mater.*, 17 (2010) 579.
36. N.Y. Zhang, D.Z. Zeng, Z.M. Yu, W.T. Zhao, J.Y. Hu, W.L. Deng, G. Tian, *Int. J. Electrochem. Sci.*, 13 (2018) 4489.
37. H.B. Xue, Y.F. Cheng, *Corros. Sci.*, 53 (2011) 1201.
38. X. Chen, C. Li, N. Ming, C. He, *J. Nat. Gas. Sci. Eng.*, 88 (2021) 103815.
39. P.F. Ying, X.Y. Li, W.P. Lu, Y.L. Chen, Z.H. Yang, B. Zhang, Y. Guo, J.F. Ding, R.K. Cao, *Int. J. Electrochem. Sci.*, 14 (2019) 8479.
40. W.S. Lyu, L.Y. Zhu, P. Yang, Z.X. Lin, Z.K. Wang, K. Wang, *Int. J. Electrochem. Sci.*, 16 (2021) 210367.
41. Z.C. Feng, X.Q. Cheng, C.F. Dong, L. Xu, X.G. Li, *J. Nucl. Mater.*, 407 (2010) 171.